Optical detection of vertical transport in GaAs/$Al_x Ga_{1-x}$As superlattices: Stationary and dynamical approaches

T. Amand, J. Barrau, X. Marie, N. Lauret, B. Dareys, and M. Brousseau
Département de Génie Physiquées, Institut National des Sciences Applique Avenue de Rangueil, 31077 Toulouse CEDEX, France

F. Laruelle
Laboratoire de Microstructures et de Microélectronique, Centre National de la Recherche Scientifique, 196 Avenue H. Ravera, Boîte Postale 107, 92225 Bagneux CEDEX, France

(Received 11 May 1992)

We propose an experimental method for the optical detection of transport along the growth axis of GaAs/$Al_x Ga_{1-x}$As superlattices (SL) that combines stationary photoluminescence excitation experiments (PLE) and time-resolved picosecond spectroscopy. We show that both the *absorption coefficient* of the structure and the *effective diffusion length* of the photogenerated excitations can be deduced from PLE experiments performed on structures with two enlarged test wells (EW) grown on both sides of the SL. The diffusion coefficients of the excitations involved in the low-temperature diffusion processes are then deduced from time-resolved experiments. A one-dimensional diffusion model is proposed taking into account two kinds of diffusive excitations: free-exciton states and localized-exciton states. We show that the capture process of the SL excitations by the enlarged wells must be taken into account in order to fit the dynamical experiments with capture times in the range 1–5 ps. The dependence of the free-exciton states's diffusion coefficient on the miniband dispersion of the structure is clearly demonstrated. Finally, temperature effects are discussed such as the influence of the free-exciton cooling on the diffusion process; the nonthermalization of the EW excitations with the lattice is also revealed.

I. INTRODUCTION

Recently, due to the continuous improvement of heteroepitaxial growth techniques, there has been a revival of interest in the field of carrier transport along the growth axis of superlattices.[1–6] For such devices, the question arises as to whether the transport properties are governed by transitions in the reciprocal space between extended Bloch type states, or by transitions in the real space between localized states.[7] When the periodicity and the interface quality are determined with an accuracy of about one monolayer, the superlattice can be viewed as a three-dimensional anisotropic semiconductor, provided that only the lower electron and hole minibands are involved in the studied processes, and that the superlattice (SL) period is short enough. More precisely, this situation occurs when the energy-transfer integral between two adjacent wells becomes higher than the energy fluctuations between them if they were considered as isolated,[8,9] in accordance with Anderson's localization criterion.[10] Several approaches have been attempted to determine transport properties of these superlattices, based on measurements performed under electric or magnetic fields.[11,12] However, in contrast with the situation in bulk semiconductor materials, some difficulties arise in the determination of the transport parameters, since the external applied fields can deeply modify the electronic states of the superlattice. For instance, when an electric field is applied to the SL, the electronic states, which are of extended Bloch type in a periodical SL without external perturbation, become localized as soon as the electrostatic potential difference between two adjacent wells becomes comparable to the miniband dispersion in energy, giving rise to the well-known Wannier-Stark ladders, as can be seen, e.g., in Ref. 13. For holes, this occurs for relatively weak electric fields; the transport properties are then modified, since they now originate from a hopping mechanism from site to site, analogously to the one described in Ref. 7.

The optical detection of vertical transport, as proposed in Ref. 4, offers the possibility of measuring the diffusion properties of the carrier motion along the growth axis, without modifying the electronic states of the structure. Based on an all optical method, it requires the preparation of a device containing the superlattice to be studied, with one or more enlarged test wells to probe the carrier population at different abscissa along the growth axis. The photoluminescence under continuous or short-pulse photoexcitation is then detected; the widths of the test wells (EW) are chosen in order to separate spectrally the SL and the EW's responses. Provided that the superlattice is thick enough to neglect the coupling between the quantum wells and the superlattice states, the transport parameters of the device can be taken as reliable values for superlattices without test wells. However, as we shall develop further, the optical method relies first on the precise knowledge of the relaxation and radiative processes in superlattice and quantum wells, particularly on the knowledge of their radiative yield; here, we shall assume that in our experimental conditions (i.e., experiments performed below about 60 K) these yields are nearly the same for both subsystems. This point can be checked experimentally and will be discussed later in Sec. III B. Second, the method requires a description of the capture

process of the electronic excitations from the superlattice to the quantum well. This point is particularly relevant in order to determine the boundary conditions of the transport equations. We shall discuss the currently used capture models, and will determine in Sec. IV a simple capture model, which is more appropriate to describe the dynamical experiments performed on such devices.

The paper is organized as follows: in Sec. II, we describe the experimental methods used in stationary and dynamical regimes to test the diffusion process in the growth-axis direction of a superlattice; in Sec. III, we present the experimental results with a qualitative analysis of vertical transport in the SL, and the model used to deduce the absorption coefficient and the diffusion length in the stationary regime; in Sec. IV, we describe the dynamical results obtained with time-resolved experiments, and develop a model in order to deduce the diffusion coefficients of the excitations involved in the transport; we show that even in the unintentionally disordered SL studied, and in addition to the diffusion of free extended Bloch-type excitons, the localized exciton states, which appear essentially because of the interface roughness inherent in the growth process, play a significant part in the diffusion process at low temperature. Finally, in Sec. V, we discuss the relationship between the two approaches, and some additional related phenomena, such as temperature effects and their influence on the diffusion process.

II. EXPERIMENT

The samples elaborated on for this study were grown by molecular-beam epitaxy under continuous growth conditions. They consist of superlattices of $GaAs/Al_xGa_{1-x}As$ with various well (L_W) and barrier (L_b) thicknesses. The superlattice thickness L was chosen to be 1 μm in all the samples. An enlarged test well of width $L_1=5$ nm has been grown on the rear side of the SL, near the GaAs substrate. A second enlarged well has been optionally grown on the opposite side of the SL near the surface. Its width, $L_2=7$ nm, has been chosen in order to separate it spectrally from the first well. The use of the configuration with two enlarged test wells, is especially useful for photoluminescence-excitation (PLE) experiments in the stationary regime, as will be seen in Sec. III. Two additional cladding layers of $Al_xGa_{1-x}As$ were grown on both sides of the whole structure in order to prevent the capture of the photogenerated excitations by the GaAs substrate, as was clearly seen in Ref. 4. The thickness of these barriers was either 50 or 100 nm. A typical sample structure with the corresponding energy-band diagram is displayed in Fig. 1(a). The various structure parameters are displayed in Table I. All the structures grown are unintentionally doped.

The PLE experiments were achieved with a pyridine-2 cw dye laser. The sample luminescence was recorded using a 0.85-m focal length Spex double monochromator, a GaAs photocathode photomultiplier, and a conventional photon counting system.

The time-resolved picosecond spectroscopy (TRS) experiments were performed using the up-conversion tech-

TABLE I. Samples structural parameters.

Sample no.	L_{clad} (nm)	L_{W_1} (nm)	L_{W_2} (nm)	L_W (nm)	L_B (nm)	x
D230	100	5	7	3.0	3.0	0.30
D228	100	5	7	2.0	2.0	0.30
D222	100	5	7	2.0	1.0	0.30
D338	50	5		3.0	4.0	0.25
D410	50	5		3.0	3.1	0.23
D314	100	5		3.0	3.0	0.25

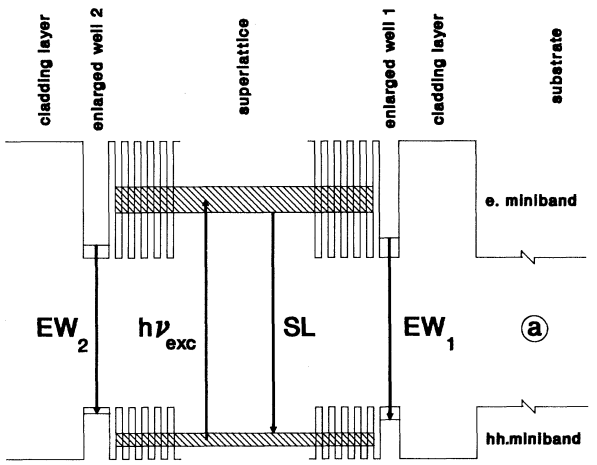

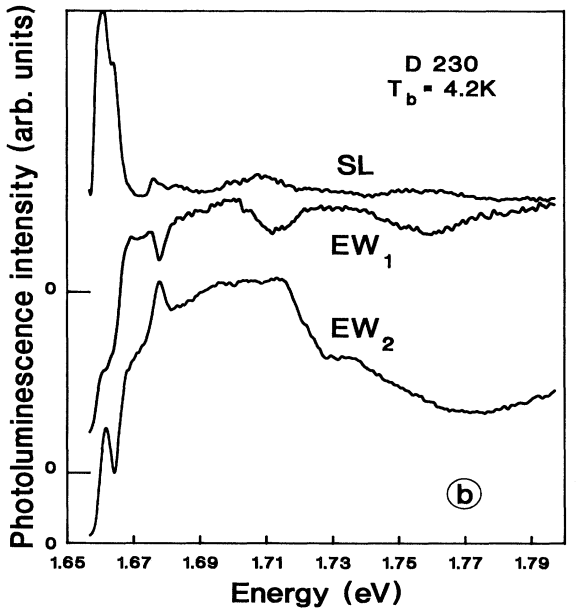

FIG. 1. (a) Energy-band diagram for a typical device containing the superlattice and two enlarged wells; the arrows indicate the optical excitation ($h\nu_{exc}$) of the radiative transitions in the SL and in the test wells (EW_1,EW_2). (b) Excitation spectroscopy of the luminescence of sample $D230$ at $T_b=4.2$ K. The detection energy of the luminescence is put at (i) 1.653 eV in the SL emission line; (ii) 1.603 eV in the EW_1 line; (iii) 1.571 eV in the EW_2 line.

nique in a $LiIO_3$ nonlinear crystal.[14,15] The excitation source was a double-jet pyridine-2 laser with a cavity dumper, synchronously pumped by the second harmonic of an actively mode-locked YAG:Nd^{3+} laser (where YAG denotes yttrium aluminum garnet). The time resolution of the system, limited here only by the dye-laser pulse duration, was about 5 ps. The frequency of the excitation pulses was chosen to be 7.6 Mhz, so that the period of operation is long with respect to the radiative lifetime in the superlattices studied; the mean excitation power was kept below 4 mW in order to create an electron-hole pair concentration below the Mott critical-density threshold, so that most of the relaxation process occurred in the excitonic regime. The absorption of the excitation beam is a one-photon process, providing a high initial electron-hole pair density gradient in the 1-μm-thick superlattices. In most experiments, the samples were put in a liquid He bath at 4.2 K, in order to minimize the nonradiative recombination processes.

III. STATIONARY EXPERIMENTS: ABSORPTION COEFFICIENT AND EFFECTIVE DIFFUSION LENGTH DETERMINATION

A. Experimental results

Figure 1(b) displays typical PLE results obtained on structures with two EW's. We detected successively the luminescence intensity in the low-energy part of the luminescence spectrum of the superlattice, corresponding to the localized exciton states, and at the emission peak of the enlarged wells [see curves labeled SL, EW_1, and EW_2, respectively in Fig. 1(b)]. The SL PLE response, recorded at 1.653 eV, shows a strong peak for a photoexcitation nearly resonant with the fundamental 1*S* heavy-hole (hh) electron (el) exciton state, at 1.661 eV. The small shoulder at 1.664 eV can be identified with the el-hh transition corresponding to the SL gap. The SL response for higher-excitation photon energy is much lower. The 1*S* light-hole (el-lh) exciton transition can be detected at 1.676 eV, followed by two weak structures at 1.710 and 1.760 eV, which will be interpreted as relaxation oscillations due to optical-phonon emission. The EW_1 test-well response displays the opposite behavior, in the sense that all the resonances appearing in the SL response appear now as antiresonances. The behavior of the EW_2 test well displays a more complex behavior: its shape resembles the absorption curve of the SL, but with the 1*s* el-hh excitonic transition strongly attenuated.

We turn now to a qualitative interpretation of these features. First of all, we describe briefly the relaxation and recombination processes in the structure. As in multiple-quantum-well systems,[14,16] the *resonantly* created el-hh excitons in the SL localize in potential fluctuations, due to structural defects of the superlattice (interface roughness, small deviations from the ideal periodicity of the SL, etc.).[4,8] Then they recombine radiatively. Practically, the exciton emission lines are slightly shifted from the absorption lines, by about 1–3 meV, toward the low energies. This can be checked from a close comparison between the PL lines, as displayed in Fig. 2, and the EW_2 PLE response, representative of the absorption of the SL, as displayed in Fig. 1 (see also Table IV for one-test-well samples). At low temperature, the free-exciton luminescence is very weak, since the localization process is much more efficient than the radiative recombination for excitons in the fundamental state [this fact can be inferred, e.g., from TRS experiments performed on high-interface-quality multiple-quantum-well systems at 4.2 K (Ref. 17)]. When the excitation is nonresonant, the electron-hole pairs created quickly form hot excitons; for our experimental conditions (weak excitation, low temperature), we assume that most electron-hole pairs are bound at the end of the excitation pulse, since its time duration is of the same order of magnitude as the exciton formation time, as can be inferred from Ref. 18. The excitons with nonzero kinetic energy cannot recombine radiatively, due to optical selection rules,[14,19,20] and thus the hot-exciton luminescence is not detected. The thermalization with the lattice, followed by the localization, is then the efficient relaxation scheme for these states. Finally, the main contribution to the luminescence in superlattices as well as in quantum wells is supplied, at low temperature, by weakly localized excitons.

As regards the transport properties of the structures studied here, two features explain why the luminescence is mostly detected in the superlattice in the case of *resonant excitation* of the SL fundamental exciton state: first, the diffusion length of these states may be much lower than the diffusion length of the hot-exciton states; second, since the absorption coefficient is large, due to the high excitonic oscillator strength, the mean distance of the photogenerated excitations from the enlarged well near the substrate (EW_2) increases. As a consequence, the PLE yield of EW_2 decreases in this spectral region, as can be seen in Fig. 1(b). Let us remark at this point that the fact that the SL PLE yield is relatively high for resonant excitation of the SL gap indicates that the formation time of bound exciton states from unbound pair states is much

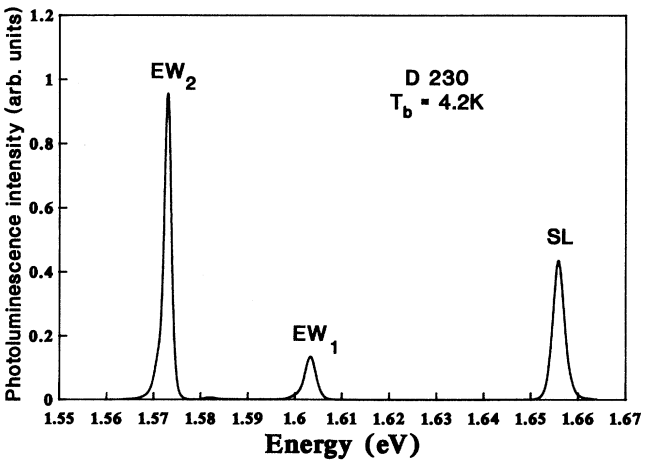

FIG. 2. Luminescence spectrum of sample *D*230 showing the relative emission intensity of the superlattice and the two enlarged wells at $T_b = 4.2$ K.

shorter than the mean escape time from the SL. The strong decrease of the SL response, in *nonresonant* excitation conditions, is due to the diffusion of the hot excitons, followed by the efficient capture by the enlarged wells. Nevertheless, a small proportion of the photocreated population relaxes its kinetic energy by emitting optical (when possible), and later acoustical phonons. The binding of the correlated electron-hole pairs into exciton states occurs at the very beginning of this thermalization process, essentially during the excitation pulse, so that the diffusion length of these unbound electron-hole pairs should be small compared to that of the hot-exciton one. The excitons finally localize and recombine radiatively. The weak el-lh excitonic peak appears because the formation time of el-hh from el-lh excitonic states its lower than, or comparable to, the mean diffusion time to escape from the superlattice [in multiple-quantum-well systems this formation time was estimated to be about 90 ps (Ref. 25)]. The relaxation oscillations appear due to a similar process: either hot excitons (or correlated electron-hole pairs) can relax down to the detected $1S$ exciton state by emitting a few optical phonons [which is achieved within about 1 ps (Ref. 19)]; the result is an enhancement of the SL response. In the other cases, if the excess kinetic energy is not an integer multiple of one of the available optical modes of the structure, the pairs must cool down (after having eventually lost most of their kinetic energy by optical-phonon emission), by acoustical-phonon emission, which is a far less efficient cooling process; the final thermalization time with the lattice is longer than the mean diffusion time to escape from the SL. Thus the observed oscillatory behavior is seen in the SL PLE spectra. We turn now to a quantitative description of diffusion in the superlattice.

B. Modelization of the stationary experiments

The purpose of this section is to give a quantitative description of diffusion in the stationary regime, based on a model as simple as possible.

First, the modelization of the diffusion process relies on the main assumption that the SL can be treated as an effective medium [when the mean kinetic energy is lower than the heavy-hole miniband dispersion, and *a fortiori* than the electron miniband dispersion, it can be viewed as an anisotropic three-dimensional (3D) material comparable to an ordered alloy]; in other words, we assume that the mean free path, l, of the diffusion elementary excitations, is small as compared to the SL thickness L:

$$l \ll L \ . \tag{1}$$

Second, since the method is based on luminescence measurements in the EW and in the SL, we make the assumption that the quantum yield η of radiative emission is the same in both subsystems, i.e.,

$$\eta_{\mathrm{SL}} \simeq \eta_{\mathrm{EW}} \ . \tag{2}$$

Third, the free-exciton formation time, from unbound electron-hole pair states at low temperature, is assumed to be of the same order of magnitude as that in quantum wells,[18] so that the diffusing excitations are mainly free excitons. This point will be checked *a posteriori* at the end of Sec. III B.

Then, calling $n(z,t)$ the local exciton concentration at time t in the SL, and labeling $0z$ the growth axis, the diffusion equation in the dynamical regime may be written in a general manner as

$$\frac{\partial n}{\partial t}(z,t) = D\frac{\partial^2 n}{\partial z^2} + \left.\frac{\partial n}{\partial t}\right|_{\mathrm{gen}} + \left.\frac{\partial n}{\partial t}\right|_{\mathrm{rec}} + \left.\frac{\partial n}{\partial t}\right|_{\mathrm{loc}} + \left.\frac{\partial n}{\partial t}\right|_{\mathrm{cap}} , \tag{3}$$

where D is the diffusion coefficient of the excitations. The generation term (neglecting the exciton formation time here) is given by the linear absorption law,

$$\left.\frac{\partial n}{\partial t}\right|_{\mathrm{gen}} = \alpha(h\nu)\Phi(0,t)e^{-\alpha(h\nu)z} , \tag{4}$$

where $\alpha(h\nu)$ is the absorption coefficient of the SL at the excitation frequency, and $\Phi(0,t)$ is the net internal photon flux at the SL surface. The recombination term is assumed to be

$$\left.\frac{\partial n}{\partial t}\right|_{\mathrm{rec}} = -\frac{n}{\tau_R'} \tag{5}$$

where τ_R' is the free-exciton lifetime, at the equilibrium temperature, of the exciton gas. The localization term is

$$\left.\frac{\partial n}{\partial t}\right|_{\mathrm{loc}} = -\frac{n}{\tau_L'} , \tag{6}$$

where τ_L' is the SL exciton localization time at the exciton-gas temperature; it is intended here as a mean value, independent of the exciton kinetic energy. Finally, the capture law of the SL excitons by the enlarged wells is assumed to be

$$\left.\frac{\partial n}{\partial t}\right|_{\mathrm{cap}} = -\left[\sum_i c_i(z)\right] n(z) , \tag{7}$$

where $c_i(z)$ are the capture coefficients of the enlarged well EW_i $(i=1,2)$. We make the assumption that the capture is only local; in other words, we approximate the capture law by

$$\left.\frac{\partial n}{\partial t}\right|_{\mathrm{cap}}(z,t) = -\sum_i c_i J_i(z) n(z_i) , \tag{7'}$$

where the functions J_i, defined by

$$J_1(z)=1 , \quad L<z<L+L_1 , \quad J_2(z)=1 , \quad -L_2<z<0$$

$$J_i(z)=0 , \quad 0<z<L , \quad i=1,2$$

take only nonzero values on their related enlarged wells EW_i. This approximation seems justified provided that condition (1) is fulfilled, since the probability density associated with the EW states falls by several decades over a few SL periods.[4]

We must now model as simply as possible the radiative recombination processes in the SL and in the wells. From time-resolved experiments performed on test SL or

multiple-quantum-well systems comparable to the one used in the present devices, it can be shown that for an exciton temperature superior to, or of the order of, 4.2 K, due to wave-vector selection rules,[14,20] the radiative lifetime of free-exciton states is long (of the order of 1 ns) compared to the localization time (of the order of 100 ps order).[16,19] Thus, we neglect the radiative recombination process for free excitons. So, we are led to the linear differential equation in the stationary regime ($\partial/\partial t=0$):

$$D\frac{\partial^2 n}{\partial z^2}-\frac{n}{\tau'_L}=-\alpha(h\nu)\Phi(0,0)e^{-\alpha(h\nu)z}\ ,\quad 0<z<L\ . \tag{8}$$

The luminescence intensity in the SL is then determined by the equations

$$\frac{n}{\tau'_L}-\frac{n_L}{\tau}=0\ , \tag{9}$$

$$I_{\rm SL}=\int_0^L\frac{n_L(z)}{\tau_R}dz=\int_0^L\eta_{\rm SL}\frac{n(z)}{\tau'_L}dz\ , \tag{10}$$

where τ and τ_R are, respectively, the lifetime and the radiative lifetime of the localized excitons, $\eta_{\rm SL}$ is the radiative yield of the recombination process, and $I_{\rm SL}$ is the emitted photon flux integrated over all the emitting directions (4π steradians); τ and $\eta_{\rm SL}$ can be expressed as a function of τ_R and the nonradiative lifetime $\tau_{\rm NR}$:

$$\frac{1}{\tau}=\frac{1}{\tau_R}+\frac{1}{\tau_{\rm NR}}\ ;\quad \eta_{\rm SL}=\left[1+\frac{\tau_R}{\tau_{\rm NR}}\right]^{-1}\ .$$

The luminescence emitted by the quantum wells EW_i is determined by the corresponding equations

$$c_i n(z_i)L_i-\frac{n_x^i}{\tau'^i_L}=0\ , \tag{11}$$

$$\frac{n_x^i}{\tau'^i_L}-\frac{n_L^i}{\tau^i}=0\ , \tag{11'}$$

$$I_i=\frac{n_L^i}{\tau_R^i}=\eta_{\rm EW}^i\frac{n_x^i}{\tau_L^i}\ ,\quad z_1=L\ ,\quad z_2=0\ , \tag{12}$$

where n_x^i and n_L^i represent the free and localized exciton areal concentration, respectively, and we define as previously τ^i and $\eta_{\rm EW}^i$ by

$$\frac{1}{\tau^i}=\frac{1}{\tau_R^i}+\frac{1}{\tau_{\rm NR}^i}\ ,\quad \eta_{\rm EW}^i=\left[1+\frac{\tau_R^i}{\tau_{\rm NR}^i}\right]^{-1}\ ,$$

with notations similar to those used for the SL. The excitation concentration in the wells ($i=1,2$) are taken as surface densities ($i=1,2$).

In the following, we shall assume that, in our low temperature conditions, the inequality $\tau_{\rm NR}^{(i)}\gg\tau_R^{(i)}$ holds for the SL and the EW's, so that all the radiative efficiencies are close to 1 and condition (2) is automatically fulfilled. The fact that recombination is dominated by radiative processes at low temperature can be inferred from the observed strong increase of the lifetime with temperature, as can be seen for quantum wells, e.g., in Refs. 31 and 32, typically below 100 K, and which is characteristic of an intrinsic behavior. For higher temperatures, the lifetime decreases quickly as the temperature increases, the recombination being dominated by nonradiative processes, as in Ref. 32.

In order to determine the boundary conditions of the differential equation (8), we must now specify the capture law in a simple manner. Two limiting cases have been considered up to now: (i) *The test wells do not significantly modify the diffusion process.* This was the approach used in, e.g., Ref. 3. (ii) *The capture process is extremely efficient at the EW's abscissa.* This hypothesis was adopted in, e.g., Refs. 4 and 6.

In the following, we determine which capture model should be used from the experimentally observed intensity ratio $I_{\rm SL}/I_1$.

Defining the mean free-exciton concentration in the SL by

$$\bar{n}=\frac{1}{L}\int_0^L n(z)dz\ ,$$

the intensity emitted by the SL is, from (10),

$$I_{\rm SL}=\eta_{\rm SL}\frac{\bar{n}}{\tau'_L}L\ . \tag{13}$$

The luminescence of EW_1 can be evaluated from (11, 11', 12) as

$$I_1=\eta_{\rm EW}^1 c_1 n(L)L_1 \tag{14}$$

so the ratio of the two luminescent components is

$$\frac{I_{\rm SL}}{I_1}=\frac{\eta_{\rm SL}}{\eta_{\rm EW}^1}\frac{\bar{n}}{n(L)}\frac{L}{L_1}\frac{1}{c_1\tau'_L}\ . \tag{15}$$

In case (i), characterized by the following condition,

$$D\frac{\partial^2 n}{\partial z^2}\bigg|_{z_i}\gg c_i n(z_i)\ ,$$

the diffusing excitations go through the wells if $0<z_i<L$ or, in our present case, are reflected by the thick barriers of $Ga_xAl_{1-x}As$ without significant capture losses by the wells. Due to the generation profile, the diffusion process occurs from the surface toward the deeper well EW_1, so that the free-exciton concentration n is a decreasing function of the abscissa z. (We neglect here, in fact, the contribution of the reflected excitations to n, assuming that the diffusion length is smaller than the SL thickness, as can be checked later.) The following inequality then holds:

$$n(z)>n(L)\ ,\quad 0<z<L\ .$$

In case (ii), the capture process is so strong that the exciton population at the well abscissa can hardly build up, ensuring that the above inequality is *a fortiori* valid. The following inequality then holds for *both cases:*

$$\bar{n}\geq n(L)\ . \tag{16}$$

As can be seen in Fig. 2 which represents the luminescence of the *a priori* less diffusive device with two en-

larged wells (*D*230), we observed an experimental ratio satisfying $I_{SL}/I_1 \lesssim 3$. This ratio is less than 1 for the other devices. Taking $L/L_1 = 200$, and $\eta_{SL}/\eta^1_{EW} \simeq 1$ at low temperature, we obtain from Eq. (15) and inequality (16) the condition

$$\frac{1}{c_1} < 1.5 \times 10^{-2} \tau'_L \ .$$

From time-resolved experiments, performed on similar test superlattices without enlarged wells, we have measured that the localization times τ'_L are in the range 100–350 ps;[19] so we obtain the following inequality for the capture time:

$$c_1^{-1} \lesssim 5 \text{ ps} \ .$$

Let us note that this inequality is consistent with the observed capture times of excitations in an alloy barrier by a quantum well.[21,22] Here, this result was suggested by the strong emission intensity, even at 4.2 K, recorded from the EW's. The capture time c_1^{-1} is lower than all the characteristic times, observed in time-resolved experiments (cf. Figs. 6–9), of the diffusion-relaxation-recombination processes.

So, we can now conclude, from the above estimations, that assumption (ii) is valid, i.e., *the capture process is extremely strong at the EW abscissa.*

In stationary experiments, the density gradient can build up during an arbitrary long time from the laser switching on; consequently, we can approximate the capture time in our model by

$$c_i^{-1} \simeq 0 \ . \tag{17}$$

It follows immediately in this case that the exciton concentration at the well abscissa must be

$$n(z_i) = 0 \ , \quad i = 1,2, \ , \tag{18}$$

as the condition

$$\lim n(z_i) = 0$$

$$c_i^{-1} \to 0$$

must be satisfied to avoid divergences in Eqs. (11) and, more generally, in Eq. (7). The generation term in these equations can then be evaluated using the particle conservation law applied at the interface between the SL and the EW_i ($i = 1,2$), and Eqs. (11) can be rewritten as

$$(-1)^i D \frac{\partial n}{\partial z}\bigg|_{z_i} - \frac{n_x^i(z_i)}{\tau'^i_L} = 0 \ , \quad i = 1,2 \ , \tag{19}$$

where we have supposed that no particles are reflected by the cladding $Ga_xAl_{1-x}As$ barriers.

We can now solve analytically the diffusion equation in the SL (8), with the conditions (18). The luminescence escaping from each region of the device can then be deduced. The results are given in Appendix A. It can easily be shown, then, that defining the diffusion length L_d as

$$L_d = \sqrt{D\tau'_L} \ , \tag{20}$$

we obtain the system of two equations

$$\frac{I_1}{I_2}(h\nu) = f(\alpha, L_d) \ , \tag{21}$$

$$\frac{I_{SL}}{I_2}(h\nu) = g(\alpha, L_d) \ , \tag{22}$$

where f and g, as defined in Appendix A, are functions of the absorption coefficient at the excitation wavelength, and of the diffusion length L_d. Since the luminescence amplitude ratios defined here are deduced experimentally from PL and PLE experiments (the PLE intensity ratios are adjusted so that they coincide with the PL ratios at the PL excitation wavelength), we can solve the implicit equation system (21) and (22) to deduce the two parameters α and L_d. This was done numerically, and the results are presented in Fig. 3, for the device *D*230. We see that the absorption curve of the superlattice is correctly reconstructed, and displays all the characteristic features, namely the el-hh 1*S* exciton transition at 1.661 eV, the el-hh 2*S* not fully resolved from the el-hh gap at 1664 eV, the el-lh 1*S* exciton at 1.677 eV; the decrease of the absorption, at 1.73 eV, corresponds to the el-hh zone-edge transition, while the small hollow structure, at 1.78 eV, could correspond to the zone-edge el-lh transition: the excitonic enhancement factor decreases quickly as soon as the exciton energy becomes higher than the minizone-edge gap. From this spectrum we can deduce the exciton binding energy to be: $E_x^b \simeq 4.6$ meV, in agreement with our estimation from exciton theory in an anisotropic semiconductor (cf. Sec. V), and with the varia-

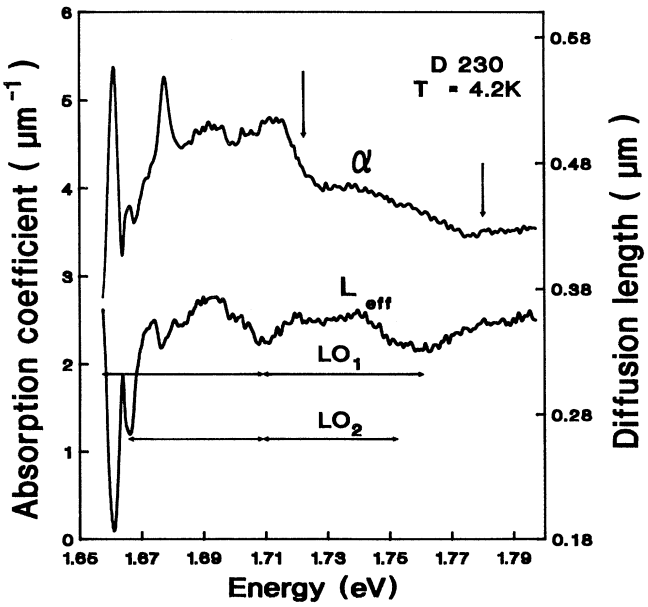

FIG. 3. Absorption coefficient (in μm^{-1}) and diffusion length (in μm) of sample *D*230 deduced from the stationary model (see text). The vertical arrows indicate the el-hh and the el-lh optical transitions at the SL minizone edge, according to the Krönig and Penney model.

tional calculations of Ref. 23. The hh-lh splitting of about 16 meV confirms the anisotropic character of the superlattice. The sum of the el and hh miniband widths deduced from the absorption curve amounts to about $\Delta_{e,h} \simeq 51$ meV; similarly, for the sum of the el and hh miniband widths, we find $\Delta_{e,\mathrm{lh}} \simeq 110$ meV. These results are in reasonable agreement with a simple Krönig and Penney calculation (see vertical arrows in Fig. 3). The diffusion-length dependence on the excitation photon energy, deduced from the model, can be roughly analyzed in two domains: In the excitonic region, the diffusion length displays antiresonances corresponding to the resonances observed in the absorption curve. The diffusion length of the lowest exciton state is relatively low—$L_d \simeq 0.2$ μm. At higher energy ($h\nu \gtrsim 1.68$ eV), the diffusion length is larger, oscillating around a plateau value of 0.35 μm. The light-hole antiresonance is weak. Then, two relaxation oscillations clearly appear, with a spectral periodicity of $P_1 \simeq 51$ meV, modulating slightly the high-energy diffusion length. The samples with lower spatial periods, $(L_W + L_B)$, have a similar general behavior, as can be seen in Figs. 4 and 5. However, the absorption is modulated by internal interferences within the devices, as is clear in Fig. 5. Moreover, the el-lh 1S exciton is nearly resonant with the el-hh gap, so the relative amplitudes of the heavy and light oscillator strength do not appear simply on the absorption curve; as a consequence, the different excitonic structures are hardly resolved on the diffusion-length curve. Finally, relaxation oscillations have a more complex structure: two systems of periodic oscillations are now superposed, the first one with the previous period $P_1 \simeq 51 \pm 1$ meV, the second one with a smaller period of $P_2 \simeq 43 \pm 1$ meV, but starting now from the el-hh gap of the SL. Two relaxation schemes are invoked to explain these oscillations. In the first one, the photogenerated electron-hole pairs quickly bind together

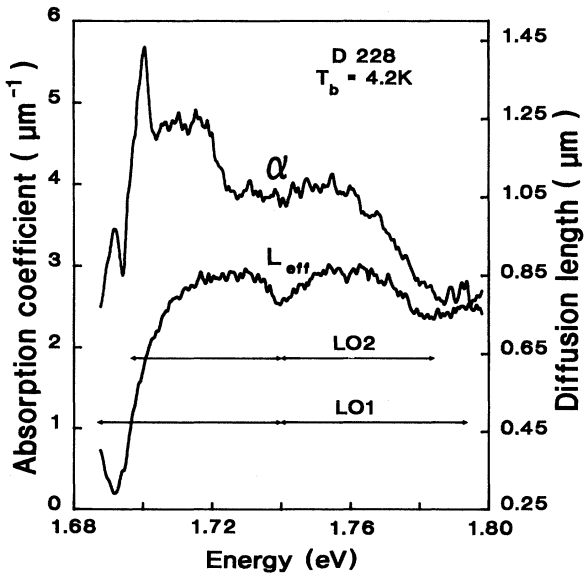

FIG. 4. Same as Fig. 3, sample $D228$.

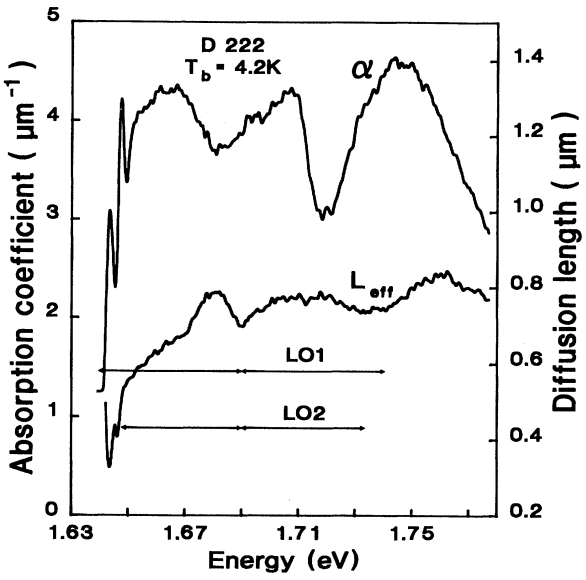

FIG. 5. Same as Fig. 4, sample $D222$.

to form a bound 1S state, emitting a LO-phonon mode of the structure; the formed excitons lose their kinetic energy by emitting LO phonons down to their dispersion curve; the oscillations appear due to the competition between the diffusion process and the cooling process, as explained in Sec. III A with a period given by

$$\hbar\omega_m = E_X + m\hbar\omega_{\mathrm{LO}_1}, \quad m = 1,2,\ldots, \tag{23}$$

where E_X corresponds to the detected exciton energy (here in the localized exciton density-of-state tail). In the second one, the electron of the photogenerated pairs lose their kinetic energy directly by emitting LO phonons down to the el conduction band; then they quickly form excitons that localize down to the detected exciton states; a minimum will appear in the diffusion length whenever this relaxation process is competitive with the diffusion process, i.e., for the excitation frequencies given by

$$\hbar\omega_n = E_G + n\left[1 + \frac{m_e}{m_{\mathrm{hh}}}\right]\hbar\omega_{\mathrm{LO}_2}, \quad n = 1,2,\ldots, \tag{24}$$

where E_G corresponds to the el-hh gap of the SL, and m_e and m_{hh} to the effective masses of the electrons and holes, respectively, in a direction parallel to the SL layers. Taking for the LO_2 mode frequency the GaAs LO-phonon mode: $\hbar\omega_{\mathrm{LO}}(\mathrm{GaAs}) \simeq 36$ meV, and $m_e \simeq 0.0665$, $m_{\mathrm{hh}} \simeq 0.34$, we find that $P_2 \simeq 43.0$ meV, in quite satisfying agreement with the experimental value reported above. For the first oscillation subset, the oscillations must coincide with a LO optical mode of the structure. We find that only the AlAs LO-phonon mode, reported at 50.2 meV,[24] could correspond to the period P_1. This is somewhat surprising, as we would have expected an AlAs-type LO mode of the barrier, which has been reported at 46.4 meV for an alloy concentration of $x \simeq 0.3$.[24] This fact is not yet completely understood and

TABLE II. Calculated effective masses in the transport direction, diffusion lengths at the 1*S* fundamental-state energy and for nonresonant excitation conditions (plateau value) deduced from the stationary model developed in Sec. III.

Sample	*D*230	*D*228	*D*222
period (nm)	6.0	4.0	3.0
$m_{e\perp}$	0.101	0.085	0.077
$m_{hh\perp}$	1.088	0.538	0.413
$m_{lh\perp}$	0.113	0.105	0.100
$L_{x,\text{eff}}$ (μm)	0.18	0.25	0.3
L_{eff} (μm)	0.35	0.85	0.80

needs further investigation. The appearance of the two types of relaxation cascades proves the coexistence of the two types of electron-hole pairs: unbound and bound excitonic states. However, the exciton cascade dominates the electron one, which confirms *a posteriori* our assumption that most electron-hole pairs are in bound excitonic states. Let us add that the electron cascade can hardly bet detected in sample *D*230; this can be attributed to the fact that electron-hole correlations in this sample are slightly higher, due to its more pronounced 2D character (the hh-lh splitting of 16 meV is the highest of this sample series).

We have summarized the main results of this section in Table II. The concluding remarks are that the diffusion length increases when the period of the SL decreases, as expected. The diffusion length of resonantly created excitons is lower, by a factor of about two, than the diffusion length of nonresonantly created ones. The further determination of the diffusion coefficients necessitates dynamical measurements which we present in the following section.

IV. DYNAMICAL TIME-RESOLVED EXPERIMENTS: THE DETERMINATION OF THE DIFFUSION COEFFICIENTS

A. Experimental results

The time-resolved experiments were performed at low temperature in nonresonant excitation conditions. Figs. 6 and 7 display the transient behavior of a two-well sample. Figs. 8 and 9 display the transient response of one-test-well structures. All the transient luminescence curves show roughly the same aspect: the rising part corresponds to the relaxation of the hot excitons, which are formed essentially during the excitation pulse, and are not radiatively active, due to selection rules; when they are thermalized to the lattice, excitons quickly localize in the potential fluctuations induced by interface roughness; they can now recombine radiatively; thus, the luminescence culminates roughly at the end of the thermalization process and then decreases due to radiative recombinations. This relaxation-recombination scheme approach is similar to the one adopted successfully in Ref. 25 for multiple-quantum-well systems, and corresponds to a simplified treatment of the one we previously determined

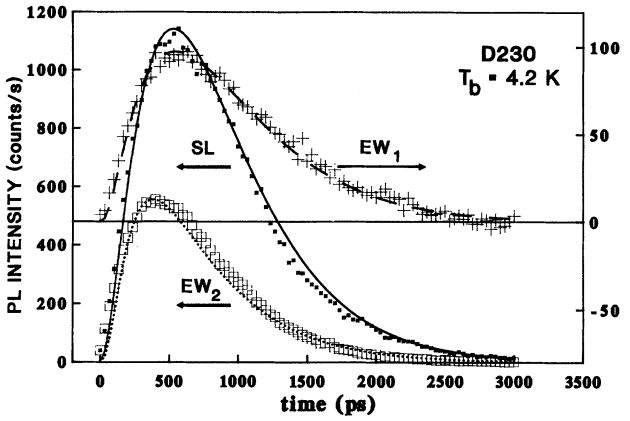

FIG. 6. Time-resolved luminescence intensities of the emission lines of a two-enlarged-wells structure (sample *D*230); SL: (■); EW_1: (+), EW_2: (□). The lines represent a fit obtained with the model described in Sec. IV (for the parameters, see Tables III and V).

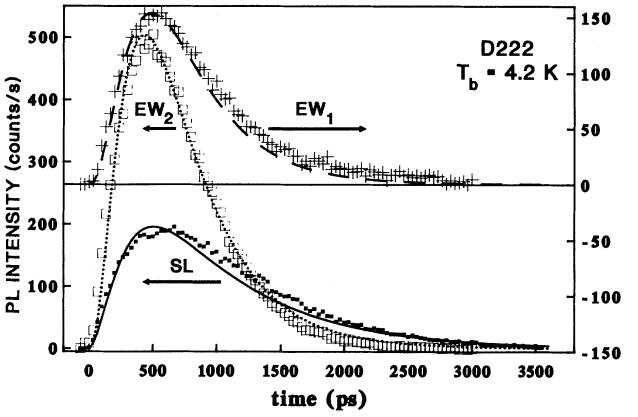

FIG. 7. Same as Fig. 6, sample *D*222.

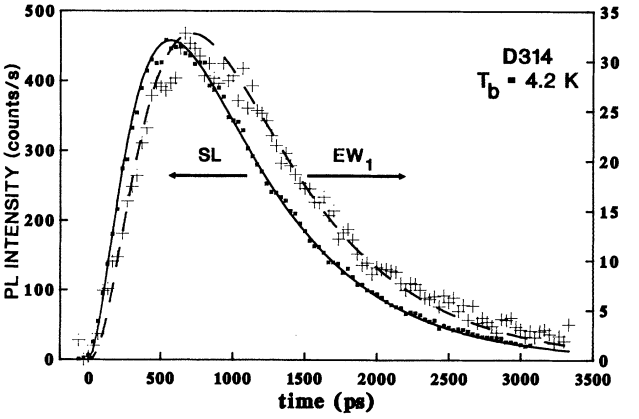

FIG. 8. Time-resolved luminescence intensities of the emission lines of a one-enlarged-well structure (sample *D*314); SL: (■), EW_1: (+). The lines represent a fit with the model described in Sec. IV (see Tables III and V).

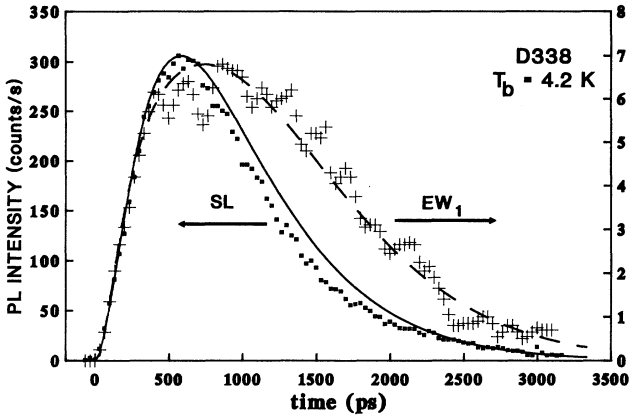

FIG. 9. Same as Fig. 8, sample *D*338. Here, the capture process dominates the diffusion process in the EW response at early time delays. Experimental data: SL, (■); EW_1(+).

in Ref. 16. We checked, by independent experiments performed on test SL or quantum wells, that the simplest model to account for the luminescence kinetics in the excitonic regime requires the use of a three-excited-level system representing, respectively, the hot-exciton states, the fundamental-exciton state, and the localized-exciton states. The transition rates between the different levels are described by first-order kinetics. This yields a simple and efficient description of the kinetic-energy-dependent localization coefficient,[16] and leads to reasonably accurate fitting.

In the two EW structures, the surface-well EW_2 temporal response is mainly determined by the capture process of SL excitations by EW_2. This can be understood from Fig. 6, where the surface test-well luminescence intensity reaches its maximum earlier than the SL. On the contrary, the capture process is not the dominating contribution of the generation process on the backward EW_1, as can be seen in Figs. 6–8: the well response rises later than that of the SL, due to the time necessary for the diffusing excitations to reach the backward EW. However, if the diffusion length is too short (cf. Fig. 9), the EW_1 signal rises again very quickly (as fast as the SL one, in normalized representation), being dominated by the capture process at short time delays, the diffusing excitations reaching the EW later (compare Figs. 8 and 9). In most cases, the luminescence of the EW's decays with a fall time much longer than their own decay time (measured independently on test wells of the same width), and is comparable to the SL fall time. This suggests that the diffusion process goes on during the last step of the SL transient regime, i.e., when excitons have relaxed their kinetic energy and are localized.[26] The time delay between the SL and the EW_1 luminescence trailing edges depends both on the absorption coefficient and on the diffusion coefficients of the SL excitations: it increases while the absorption coefficient increases, since then the mean distance of the generated excitation from EW_1 increases. So, this time delay reflects the conjugated action of these two parameters and is not directly representative of the diffusion properties of a given structure. For very short-period SL's, the initial diffusion of free excitons dominates the final diffusion of the localized states, so that the EW's signal fall time becomes shorter than the SL one, partly reflecting their own decay time. As in stationary experiments, the luminescence instantaneous intensity ratios $I_1/I_2(h\nu,t)$ and $I_{SL}/I_2(h\nu,t)$ are determinant parameters, but here again, they depend both on the absorption coefficient $\alpha(h\nu)$ and on the diffusion coefficient. In fact, a detailed calculation, taking into account all the previously mentioned effects, is required to determine the SL transport properties, as we shall see now.

B. The low-temperature dynamical model

We give here a description of the diffusion process at low temperature in the superlattice (the temperatures of the excitations here are typically in the range $T \lesssim 40$ K). As was stated in Sec. IV A, three kinds of elementary excitations take part in the diffusion process, namely the hot-excitonic states, the fundamental-, and the localized-excitonic states of respective densities $n_{X,H}$, n_X, n_L. We face now a system of three coupled differential equations:

$$\frac{\partial n_{X,H}}{\partial t} = D_{X,H}\frac{\partial^2 n_{X,H}}{\partial z^2} + \alpha\Phi(z,t) - \frac{n_{X,H}}{\tau_{\rm th}} , \tag{25}$$

$$\frac{\partial n_X}{\partial t} = D_X\frac{\partial^2 n_X}{\partial z^2} + \frac{n_{X,H}}{\tau_{\rm th}} - \frac{n_X}{\tau_L} , \tag{26}$$

$$\frac{\partial n_L}{\partial t} = D_L\frac{\partial^2 n_L}{\partial z^2} + \frac{n_X}{\tau_L} - \frac{n_L}{\tau_R} , \tag{27}$$

where $\tau_{\rm th}$, τ_L, and τ_R represent, respectively, the thermalization time of the hot excitons to the lattice temperature, the localization time of excitons in their fundamental state, and the radiative lifetime of localized excitons.

In such a model, we made the following approximations.

(i) The unbound correlated pairs are neglected, the binding process being mostly achieved during the excitation pulse (the associated diffusion length should be shorter than that of the other excitations, which will be checked *a posteriori*).

(ii) The only efficient radiative process comes from the recombination of localized exciton states, in our low-excitation-density conditions.

(iii) The capture by the wells is described as in the stationary experiments: we consider it as local and strong. But, in the dynamical regime, we must now take the capture time into account, to model the luminescence rise in the EW's.

(iv) There is no surface recombination at the interface between the SL and the $Ga_xAl_{1-x}As$ front cladding layer, nor at the interface between one EW and its adjacent cladding layer, so the particle current density is zero through these planes.

The boundary conditions of the differential system are then determined by the following differential system:

$$\frac{\partial n_{X,H}}{\partial t}(z_i,t)=(-1)^i\frac{D_{X,H}}{L_i}\frac{\partial n_{X,H}}{\partial z}(z_i,t)-c_i n_{X,H}(z_i,t)\ ,$$

$$\frac{\partial n_X}{\partial t}(z_i,t)=(-1)^i\frac{D_X}{L_i}\frac{\partial n_X}{\partial z}(z_i,t)-c_i n_X(z_i,t)\ , \tag{28}$$

$$\frac{\partial n_L}{\partial t}(z_i,t)=(-1)^i\frac{D_L}{L_i}\frac{\partial n_L}{\partial z}(z_i,t)-c_i n_L(z_i,t)\ ,$$

$$i=1,(2)\ ,$$

where we have supposed, for the sake of simplicity, that the capture coefficients are independent of the exciton energy. Finally, the initial particle distributions before the excitation optical pulse are given by

$$n_{X,H}(z,t_0)=0,\quad 0\le z\le L\ ,$$

$$n_X(z,t_0)=0,\quad 0\le z\le L\ , \tag{29}$$

$$n_L(z,t_0)=0,\quad 0\le z\le L\ .$$

The time origin t_0 has been chosen before the excitation pulse, so that no hypothesis is made on the initial profile.

The differential-evolution equations of the exciton population in the quantum wells are given by

$$\frac{\partial n^i_{X,H}}{\partial t}=c_i L_i[n_{X,H}(z_i,t)+n_X(z_i,t)+n_L(z_i,t)]-\frac{n^i_{X,H}}{\tau^i_{\rm th}}\ , \tag{30}$$

$$\frac{\partial n^i_X}{\partial t}=\frac{n^i_{X,H}}{\tau^i_{\rm th}}-\frac{n^i_X}{\tau^i_L}\ , \tag{31}$$

$$\frac{\partial n^i_L}{\partial t}=\frac{n^i_X}{\tau^i_L}-\frac{n^i_L}{\tau^i_R}\ , \tag{32}$$

where the capture occurs via the hot-exciton states of the quantum wells.

The luminescence intensity is given in each region as before by

$$I_{\rm SL}(t)=\int_0^L\frac{n_L(z,t)}{\tau_R}dz\ , \tag{33}$$

$$I_i(t)=\frac{n^i_L(t)}{\tau^i_R}\ ,\quad i=1,(2)\ . \tag{34}$$

The differential system (25)–(27) has been solved numerically together with the boundary conditions (28), using an implicit algorithm with unconditional stability. Practically, the optical pulse envelope has been taken as a Gaussian pulse, with a full width at half maximum $\Delta t\simeq 5$ ps estimated by an autocorrelation measurement performed on the excitation beam, and the origin t_0 at $5\Delta t$ before the optical pulse maximum. The instantaneous luminescence intensity is deduced at each temporal step of the simulation. The results are displayed in Figs. 6–9, together with the experimental results. Despite the numerous parameters involved in the model, the critical parameters are the absorption coefficient at the excitation photon energy $\alpha(h\nu_{\rm ex})$ and the diffusion coefficients $D_{X,H}$ for the intensity ratios, and D_L for the trailing edge of the EW luminescence; the fit is much less sensitive to the D_X coefficient, since the corresponding diffusion length L_X is much shorter than the diffusion length of hot excitons, $L_{X,H}$. The order of magnitude of the thermalization, localization, and radiative recombination times ($\tau_{\rm th}$, τ_L, τ_R, respectively) can be estimated from separate time-resolved measurements of the luminescence kinetics on a test superlattice (without EW, but with cladding layers), and of the luminescence of the EW's excited selectively with a photon energy just below the gap of the SL (or of the test multiple-quantum-well structures with the corresponding structural parameters). So, one can consider that only five (six) adjustable parameters are to be determined for structures with one (two) enlarged wells: $D_{X,H}$, D_X, D_L, α, c_1 (c_2). We now have to describe the capture process more accurately than we did in Sec. III B, in order to be able to use the measured relaxation parameters of the test structures without significant modification to the diffusion model. The obtained results are displayed in Figs. 6–9. Let us stress again the fact that we fit not only the temporal shapes of the SL and the EW, but also their *relative intensities*. Thus, five (eight) independent characteristic parts of the kinetics must be described: the rising and falling parts of the transient luminescence of the SL

TABLE III. Calculated effective masses in the transport direction, absorption coefficients, diffusion length of hot excitons, fundamental-state excitons, and localized-state excitons deduced from the dynamical model developed in Sec. IV.

Sample	*D*230	*D*228	*D*222	*D*338	*D*314	*D*410
p (nm)	6.0	4.0	3.0	7.0	6.0	6.1
$m_{e\perp}$	0.101	0.085	0.077	0.104	0.091	0.088
$m_{\rm hh\perp}$	1.088	0.538	0.413	1.305	0.791	0.732
$m_{\rm lh\perp}$	0.113	0.105	0.100	0.114	0.108	0.106
$m_{e\perp}+m_{\rm hh\perp}$	1.189	0.623	0.490	1.409	0.882	0.820
α (10^4 cm^{-1})	2.0	1.2	2.0	4.2	3.2	3.0
$L_{X,H}$ (μm)	0.19	0.35	0.49	0.15	0.20	0.23
L_X (μm)	0.09	0.14	0.19	0.08	0.12	0.11
L_L (μm)	0.09	0.20	0.13	0.4	0.19	0.11
$D_{X,H}$ (cm^{2}s^{-1})	0.8	2.4	4.0	0.53	1.5	1.3
D_X (cm^{2}s^{-1})	0.5	1.4	2.5	0.53	1.2	1.0
D_L (cm^{2}s^{-1})	0.2	0.2	0.2	0.53	0.5	0.2

and of EW_1 (EW_2), and the peak intensity ratios $I_{SL}/I_1(I_{SL}/I_2)$. We fit the experimental data with reasonably good accuracy. The diffusion parameters deduced from the fit are summarized in Table III while the corresponding characteristic relaxation and recombination times used are reported in Table V (Appendix B).

We observe the following general trends.

(i) The diffusion coefficients depend critically on the barrier thicknesses: they decrease quickly when L_B increases, especially for the hot excitons.

(ii) The absorption coefficient increases with the barrier thickness. This corresponds to the increase of the 2D character of the electronic states of the SL, leading to a higher transition oscillator strength. However, we notice that the two-well samples yield slightly lower absorption coefficients than the one-well samples for comparable exciton masses; we attribute this fact to the approximate character of the diffusion model.

(iii) The excitonic diffusion lengths deduced from dynamical experiments are in reasonable agreement with the ones deduced from stationary experiments, although the latter take higher values. We will come back to this point in the following discussion.

V. DISCUSSION AND CONCLUSION

From both stationary and dynamical experiments, it clearly appears that the diffusion lengths increase when the exciton effective mass decreases; the main contribution to this is the hh effective-mass variation with the SL period, the other effective masses (el and lh) being far less sensitive to the SL period in the observed structural parameter range. The same correlation appears for the diffusion coefficients. So the diffusion process seems controlled by the heavy-hole effective mass. We discuss now some corollary transport properties.

A. Temperature effects

We neglected in the preceding sections the effect of temperature on the diffusion processes, and on the localization process of bound pairs. Figure 10 shows the increase of the diffusion process when the temperature of the system is raised in the stationary regime. Two regimes can be distinguished: first, the ratio of I_1/I_{SL} increases slowly, as the temperature of the device is increased; then, above about 14 K, it increases more quickly. The two regimes can be described by two activation energies, which are cited in Table IV. As can be seen from spectroscopic data, the first process can be attributed to the detrapping of the localized exciton states. This process is similar to the one observed in multiple-quantum-well systems by resonant Rayleigh scattering.[30] The second activation energy may be attributed to the population of the light-hole 1S exciton subband, whose states can contribute efficiently to the diffusion due to their lower effective mass.

TABLE IV. The activation energies deduced from the stationary temperature-dependent experiments compared to the exciton "Stokes shift" and heavy-hole–light-hole splitting recorded on spectroscopic experiments.

	p (nm)	m_{hh}	ΔE_1 (meV)	Δ_s (meV)	ΔE_2 (meV)	Δ_{lh} (meV)
D338	7.0	1.3	3.2	2.4	17.6	17.2
D410	6.1	0.732	1.4	1.5	11.6	11.7

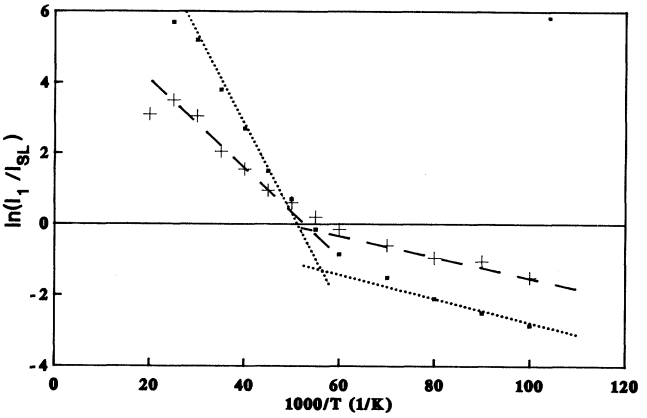

FIG. 10. Temperature dependence of the intensity ratio of the luminescence in the enlarged well and in the superlattice, for the three one-well samples (see Table I), in the stationary regime. Experimental data: $D338$, (■); $D410$, (+). For a given sample, the two activation energies (see text) are deduced from the represented straight lines.

Figure 11 shows the temperature evolution at the beginning of the kinetics in the dynamical regime, measured from the high-energy tail of the localized-exciton

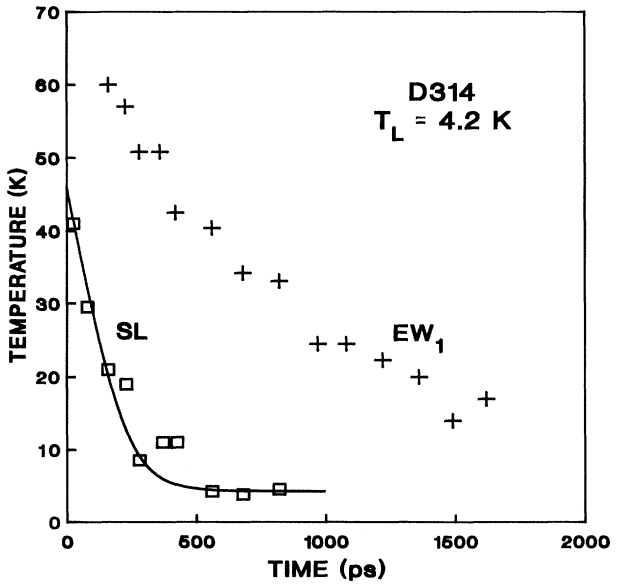

FIG. 11. Dynamical behavior of the temperature in the $D314$ sample, obtained from time and spectral resolved spectroscopy measurements. SL: (□), EW_1: (+). Note that the quantum well is not thermalized with the SL.

luminescence spectra, both in the superlattice and in the enlarged well, in sample *D*314. The initial exciton temperature in the SL is about 40 K, in agreement with the position of the onset of optical processes in the theoretical exciton cooling curve displayed in Fig. 12, and decreases down to the lattice temperature in about 500 ps. The exciton cooling model relies on a generalization of 3D exciton cooling,[27] the SL being treated as a 3D anisotropic material; we have adopted the spherical approximation for the 1*S* exciton wave function, which is valid up to the second order of perturbation theory, as developed in Ref. 28, using the effective masses quoted in Table II. This approach yields results, for the exciton binding energy, comparable to the ones determined by the variational computation approach used in Ref. 23, in the limit of short-period superlattices. The SL exciton cooling model is computed with the material parameters used in Ref. 16; it fits the experimental data with *no* adjustable parameters (the temperature of the exciton system just after the excitation pulse being measured directly).

The temperature in the EW has a similar behavior, but takes higher values than in the SL, even at long time delays: this is due to the fact that the diffusion-generated excitations in the EW have a high initial kinetic energy; most of this is dissipated by LO-phonon emission, but the remaining kinetic energy cannot be fully dissipated by acoustical-phonon emission during the excitation lifetime; as was seen in Ref. 16, the onset of the LO-phonon emission in the cooling curve occurs at somewhat higher temperatures in quantum wells than in three-dimensional systems, which explains qualitatively the higher initial temperature in the EW. The exciton system in the EW does not thermalize with the lattice during its lifetime, which supports the fact that diffusion of localized-exciton states occurs in the SL at long time delays. The basic mechanism that can be invoked here is the hopping (eventually assisted by acoustical-phonon emission) between these localized states, yielding a particle current along the growth axis toward the EW's, through processes similar to the one reported in Ref. 29 to describe the spectral diffusion of localized-exciton states in quantum wells.

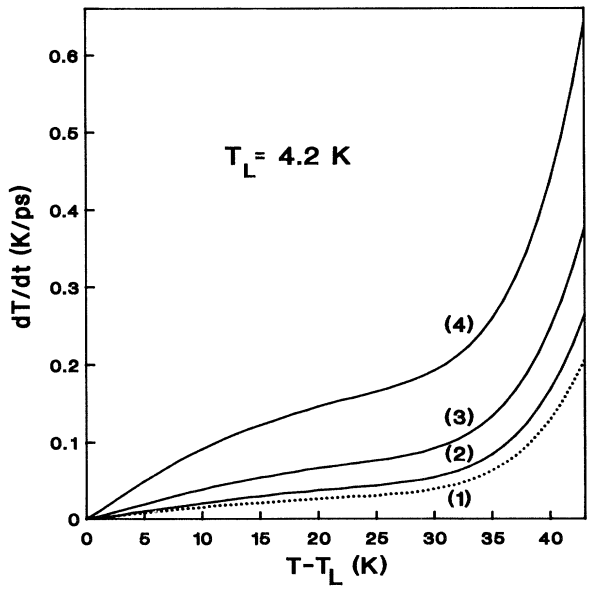

FIG. 12. Exciton cooling rate for different superlattice vertical heavy-hole exciton masses as a function of the exciton temperature. The lattice temperature is $T_L = 4.2$ K. Three processes are taken into account: acoustical deformation potential, piezoelectric, and polar optic. The onset of the polar optic process is clearly seen about 35–40 K. (1) Bulk GaAs; (2) *D*222; (3) *D*228; (4) *D*314.

To conclude, one can say that a full diffusion calculation should include the temperature dependence of the diffusion parameters used, and two supplementary cooling equations for the SL and the EW. Thus, the diffusion parameters determined from the fit of dynamical experiments at low temperature must be interpreted as mean values in the temperature range described by the exciton system in these experiments. For temperatures higher than 15–20 K, the light-hole contribution to the diffusion process should be also included.

B. Relation between the stationary and dynamical approaches

In Sec. III, the experimental results were explained with a single diffusion equation. The dynamical experiments require, on the other hand, the use of three coupled differential equations, as three kinds of particles are involved in the diffusion process. We check now the compatibility between the two models, on the basis of the following two assumptions.

(1) The electron-hole system internal thermalization is achieved during the excitation pulse, so that bound and unbound pairs have the same temperature T, eventually higher than the lattice temperature T_L, during all the kinetics.

(ii) The localized excitons are also thermalized with the free-exciton gas; this means that the localization time used previously corresponds, in fact, to the balance between a capture rate from free to localized states, and an emission rate for the reverse process, each rate being much faster than the internal thermalization time of the free-exciton gas. This approach was used successfully in Ref. 16.

Under these conditions, the ratios between the 1*S* hot-exciton states and the localized-exciton states, r_1, as well as between the fundamental-exciton states and the localized states, r_2, are only functions of the temperature T of the exciton gas. In the stationary regime, T and thus r_i are constant. Letting

$$r_1(T)=\frac{n_{X,H}}{n_L} ,$$
$$r_2(T)=\frac{n_X}{n_L} , \tag{35}$$
$$n=n_{X,H}+n_X+n_L ,$$

and adding together Eqs. (25)–(27), we obtain, for the

stationary regime ($\partial/\partial t \equiv 0$), the diffusion equation in the SL:

$$0 = D_{\text{eff}} \frac{\partial^2 n}{\partial z^2} + \alpha \phi(z,0) - \frac{n}{\tau_{\text{eff}}} ,$$
$$0 = \frac{n}{\tau_{\text{eff}}} - \frac{n_L}{\tau_R} , \tag{36}$$

where we have defined the effective parameters as

$$D_{\text{eff}}(T) = \frac{r_1(T) D_{X,H}(T) + r_2(T) D_x(T) + D_L(T)}{r_1(T) + r_2(T) + 1} ,$$
$$T_{\text{eff}} = \tau_R (r_1(T) + r_2(T) + 1) . \tag{37}$$

We can also define the effective diffusion length as

$$L_{\text{eff}}(T) \equiv [D_{\text{eff}}(T) \tau_{\text{eff}}(T)]^{1/2} = \left[r_1(T) \frac{\tau_R}{\tau_{\text{th}}} L_{X,H}^2 + r_2(T) \frac{\tau_R}{\tau_L} L_X^2 + L_L^2 \right]^{1/2} . \tag{38}$$

The luminescence is always defined by Eq. (10) in the SL. Similarly, as the quantum-well total density is defined by

$$r_1^i(T) = \frac{n_{X,H}^i}{n_L^i} ,$$
$$r_2^i(T) = \frac{n_X^i}{n_L^i} , \tag{39}$$
$$n^i = n_{X,H}^i + n_X^i + n_L^i ,$$

we obtain, neglecting the excitation concentrations at both extremities of the SL ($n(z_i) \simeq 0$, $i = 1,2$) as in Sec. III B, the effective equations

$$0 = (-1)^i D_{\text{eff}} \frac{\partial n}{\partial z}(z_i) - \frac{n^i}{\tau_{\text{eff}}^i} ,$$
$$0 = \frac{n^i}{\tau_{\text{eff}}^i} - \frac{n_L^i}{\tau_R^i} , \tag{40}$$

with the notation

$$\tau_{\text{eff}}^i = \tau_R^i (r_1^i(T) + r_2^i(T) + 1) . \tag{41}$$

The luminescence intensity is given by Eq. (10) in the SL and by Eq. (12) in the EW, as before. So, by identifying D and D_{eff}, τ_L' and τ_{eff}, and L_d and L_{eff}, we obtain a differential system exactly equivalent to the system (8)–(12). Clearly,

$$\lim r_i(T) = 0 , \quad T \to 0$$

we have in this limit

$$D_{\text{eff}}(T) \sim D_L(T) ,$$
$$L_{\text{eff}}(T) \sim L_L(T) . \tag{42}$$

So, we can reinterpret the stationary experiments: first, the absorption coefficient computation is unmodified so that the absorption curves, deduced from the stationary model in Sec. III, are correct. Second, the diffusion-length curves, deduced in the latter model, must be interpreted as effective diffusion-length spectra. The spectral variations of L_{eff} are mainly attributed to the relaxation processes in the exciton system: for resonant excitation with the $1S$ transition, the created exciton gas is cold, at the lattice temperature, so the measured L_{eff} coincides with L_X at low temperature [see Eq. (38), $T_L \simeq 4.2$ K]. As the photon energy increases, the temperature of the system increases, so that the hot-exciton population rises, and the effective diffusion length increases according to (38). Then the temperature saturates when the LO-optical-phonon emission process becomes efficient, i.e., comparable to or higher than the acoustical-phonon emission process; the thermal threshold for LO-phonon emission has been determined to be about 40 K as discussed in Sec. V A and as can be seen in Fig. 12. So, the general behavior of the diffusion length reflects the electronic temperature of the system. The relaxation oscillations can be interpreted within this framework since, for excitations at phonon energies defined by (23) or (24), efficient cooling channels by LO-phonon emission lead to a cooler electron-hole system.

Finally, it can be noted that the diffusion length and the absorption coefficient determined in stationary experiments are somewhat overestimated with respect to those determined in dynamical experiments. We have verified that introducing a finite capture process in the stationary model leads to lower determinations of α and L_{eff}, yielding a better agreement; but this is done at the cost of the introduction of two adjustable parameters in Eqs. (21) and (22): c_1 and c_2. So, the simple stationary diffusion model gives the correct variations of the absorption coefficient and the diffusion length, while their absolute values are known to within a multiplicative factor of about two.

To conclude, we have performed the first systematic study of the diffusion properties of superlattices by optical detection of vertical transport, using a combined approach including stationary PLE experiments and time-resolved spectroscopy. In low excitation and temperature conditions, the transport is dominated by the exciton diffusion process; we have demonstrated that two kinds of elementary excitations participate in this process, namely free (essentially hot) excitons, which are of extended Bloch type, and localized-exciton states of limited spatial extent. The diffusion coefficient of the former depends critically on the heavy-hole effective mass, while the opposite is true for the latter.

ACKNOWLEDGMENTS

We acknowledge B. Etienne for the growing of the high-quality samples used in this study. Part of this work was supported by Région Midi-Pyrenées.

APPENDIX A

Equation (8) is first solved using the boundary conditions (18). We obtain

$$n(z)=\frac{\alpha\Phi\tau_L}{1-L_d^2\alpha^2}(Ae^{z/L_d}+Be^{(-z/L_d)}+e^{-\alpha z}) , \quad \text{(A1)}$$

with the coefficients A and B determined by (18):

$$A=\frac{e^{-L/L_d}-e^{-\alpha L}}{e^{L/L_d}-e^{-L/L_d}} ; \quad B=\frac{e^{L/L_d}-e^{-\alpha L}}{e^{-L/L_d}-e^{L/L_d}} . \quad \text{(A2)}$$

The intensity emitted by the superlattice is then, from (10),

$$I_{SL}=\frac{\alpha\Phi\eta_{SL}}{1-L_d^2\alpha^2}\left[AL_d(e^{L/L_d}-1)-BL_d(e^{-L/L_d}-1)-\frac{1}{\alpha}(e^{-\alpha L}-1)\right] . \quad \text{(A3)}$$

The intensity emitted by the EW's is obtained from (12) and (19):

$$I_1=-\frac{\alpha\Phi L_d^2\eta_{EW}^{(1)}}{1-L_d^2\alpha^2}\left[\frac{A}{L_d}e^{L/L_d}-\frac{B}{L_d}e^{-L/L_d}-\alpha e^{-\alpha L}\right] , \quad \text{(A4)}$$

$$I_2=\frac{\alpha\Phi L_d^2\eta_{EW}^{(2)}}{1-L_d^2\alpha^2}\left[\frac{A}{L_d}-\frac{B}{L_d}-\alpha\right] . \quad \text{(A5)}$$

For $\alpha=1/L_d$, expressions (A3–A5) take a different analytical form, but we have checked that n_x, I_{SL}, and I_i are continuous functions of α, so that no divergence occurs for this particular value. Assuming identical radiative yield in the EW's and in the SL, we obtain the system

$$\frac{I_1}{I_2}(h\nu)=-\frac{Ae^{L/L_d}-Be^{-L/L_d}-\alpha L_d e^{-\alpha L}}{A-B-\alpha L_d} , \quad \text{(A6)}$$

$$\frac{I_{SL}}{I_2}(h\nu)=\frac{A(e^{L/L_d}-1)-B(e^{-L/L_d}-1)-\frac{1}{\alpha L_d}(e^{-\alpha L}-1)}{A-B-\alpha L_d} \quad \text{(A7)}$$

which corresponds to the system (21) and (22).

The first ratio, corresponding to the f function (21), is mainly sensitive to the absorption coefficient, while the second one, the g function (22), to the diffusion length. As an example, we evaluate here a few limiting cases:

For $L_d/L \ll 1$, with L remaining finite, we obtain, after performing some algebra and making the appropriate Taylor expansions, the equivalent expressions

$$f(\alpha,L_d)\sim e^{-\alpha L} , \quad \text{(A8)}$$

$$g(\alpha,L_d)\sim\frac{L}{L_d}\frac{1-e^{-\alpha L}}{\alpha L} , \quad \text{(A9)}$$

$$L_d\to 0 .$$

If, moreover, the SL is weakly absorptive, i.e., $\alpha L \ll 1$, we obtain

$$f(\alpha,L_d)\sim 1-\alpha L , \quad \text{(A8')}$$

$$g(\alpha,L_d)\sim\frac{L}{L_d} , \quad \text{(A9')}$$

$$L_d , \quad \alpha\to 0 ,$$

while in a strongly absorptive material, i.e., $\alpha L \gg 1$, we obtain

$$f(\alpha,L_d)\sim e^{-\alpha L} , \quad \text{(A8'')}$$

$$g(\alpha,L_d)\sim\frac{1}{\alpha L_d} , \quad \text{(A9'')}$$

$$L_d , \quad \alpha^{-1}\to 0 .$$

In our experimental cases, α^{-1}, L_d, and L are all of the same order of magnitude, so that the full expressions must be used. However, the determination of α and L_d is accurate, since the exponential functions take values in a limited range.

APPENDIX B

We display in Table V the relaxation, localization, and radiative times used for the SL and the EW_i in the fitting of dynamical time-resolved experiments. An independent measurement performed with a pulsed laser excitation

TABLE V. The sample characteristic times used to fit the dynamical model developed in Sec. V to the experimental data. Times are given in ps.

Sample	*D*230	*D*228	*D*222	*D*338	*D*314	*D*410
m_e+m_{hh}	1.189	0.623	0.490	1.409	0.882	0.820
τ_{th}	450	500	600	425	275	400
τ_L	150	150	150	125	125	125
τ_R	450	600	900	450	750	600
τ_C^1	1	1	1	1	1	1
τ_C^2	1	2	1			
τ_{th}^1	100	100	100	50	100	100
τ_L^1	50	100	50	50	100	75
τ_R^1	350	250	350	350	350	350
τ_{th}^2	100	120	100			
τ_L^2	50	100	100			
τ_R^2	375	375	375			

with a photon energy below the SL gap yielded $\tau_{th}^1 = 100$ ps, $\tau_L^1 = 80$ ps, and $\tau_R^1 = 350$ ps for the sample $D338$. The same experiment performed on the $D336$ sample yielded $\tau_{th}^1 = 100$ ps, $\tau_L^1 = 100$ ps, and $\tau_R^1 = 280$ ps. We deduced from more accurate experiments performed on multiple-quantum-well systems with relevant structural parameters: $\tau_L^1 \simeq 100$ ps and $\tau_R^1 \simeq 375$ ps, $\tau_L^2 \simeq 100$ ps and $\tau_R^2 \simeq 350$ ps.

[1]K. Fujiwara, J. L. de Miguel, and K. Ploog, Jpn. J. Appl. Phys. **24**, L405 (1985).

[2]F. Capasso, K. Mohammed, and A. Y. Cho, IEEE J. Quantum Electron. **QE-22**, 1853 (1986).

[3]J. Benhlal, P. Lavallard, C. Gourdon, R. Grousson, M. L. Roblin, A. M. Pougnet, and R. Planel, J. Phys. (Paris) **48**, C5-471 (1987).

[4]A. Chomette, B. Devaud, J. Y. Emery, and A. Regreny, Superlatt. Microstruct. **1**, 201 (1985); A. Chomette, B. Deveaud, B. Lambert, F. Clérot, and A. Regreny, *ibid.* **5**, 403 (1989).

[5]K. Fujiwara, N. Tsukada, T. Nakayama, and A. Nakamura, Phys. Rev. **40**, 1096 (1989).

[6]J. Puls, F. Henneberger, I. N. Uraltsev, A. M. Vassiliev, Superlatt. Microstruct. **9**, 503 (1991).

[7]D. Calecki, J. F. Palmier, and A. Chomette, J. Phys. C **17**, 5017 (1984).

[8]E. Tuncel, L. Pavesi, D. Martin, and F. K. Reinhart, Phys. Rev. B **38**, 1597 (1988).

[9]A. Chomette, B. Deveaud, A. Regreny, and G. Bastard, Phys. Rev. Lett. **57**, 1464 (1986).

[10]P. W. Anderson, Phys. Rev. **109**, 1492 (1958).

[11]J. F. Palmier, C. Minot, J. L. Lievin, F. Alexandre, J. C. Harmand, J. Dangla, C. Dubon-Chevallier, and D. Ankri, Appl. Phys. Lett. **49**, 1260 (1986).

[12]T. Duffield, R. Bhat, M. Koza, F. De Rosa, D. M. Hwang, P. Grabbe, and S. J. Allen, Jr., Phys. Rev. Lett. **56**, 2724 (1986).

[13]J. Barrau, K. Khirouni, Do Xuan Than, T. Amand, M. Brousseau, F. Laruelle, and B. Etienne, Solid State Commun. **74**, 147 (1990).

[14]T. Amand, F. Lephay, S. Valloggia, M. Brousseau, and A. Regreny, Superlatt. Microstruct. **6**, 323 (1989).

[15]J. Shah, IEEE J. Quantum Electron. **QE-24**, 276 (1988).

[16]X. Marie, F. Lephay, T. Amand, J. Barrau, F. Voillot, Superlatt. Microstruct. **10**, 415 (1991).

[17]J. F. Ryan, Physica B **134**, 403 (1985).

[18]T. C. Damen, J. Shah, D. Y. Oberly, D. S. Chemla, and J. E. Cunningham, Phys. Rev. B **42**, 7434 (1990).

[19]X. Marie, Ph.D thesis, Toulouse University, 1991.

[20]S. Munnix, D. Bimberg, D. E. Mars, J. N. Miller, E. C. Larkins, and J. S. Harris, Superlatt. Microstruct. **6**, 369 (1989); J. Christen, M. Krahl, and D. Bimberg, Superlatt. Microstruct. **7**, 1 (1990).

[21]J. Feldmann, G. Peter, E. O. Göbel, K. Leo, H. J. Polland, K. Ploog, K. Fujiwara, and T. Nakayama, Appl. Phys. Lett. **51**, 226 (1987).

[22]B. Deveaud, F. Clérot, A. Regreny, K. Fujiwara, K. Mitsunaga, and J. Ohta, Appl. Phys. Lett. **55**, 2646 (1989).

[23]A. Chomette, B. Lambert, B. Deveaud, F. Clerot, A. Regreny, and G. Bastard, Europhys. Lett. **4**, 461 (1987).

[24]B. Jusserand and J. Sapriel, Phys. Rev. B **24**, 7194 (1981).

[25]J. Kusano, Y. Segawa, Y. Aoyagi, and S. Namba, Phys. Rev. B **40**, 1685 (1989).

[26]We have checked that the reabsorption of the SL luminescence by the enlarged wells yields a negligible contribution to the EW's luminescence: for optical modes propagating along the growth axis, the EW absorption is less than 1% of the incident radiation. For the modes propagating parallel to the SL layers, which are guided due to the lower refraction index in the cladding layers, the losses due to EW_i must be multiplied by the factor Γ corresponding to the overlap between the EW confined electronic states and the electromagnetic field; here we have $\Gamma < L_i/L$ so that $\Gamma \lesssim 5 \times 10^{-3}$. Since, due to our experimental technique, the analyzed area is of the order of 100 μm^2, these modes can hardly contribute efficiently to the detected EW luminescence.

[27]X. Marie, T. Amand, B. Dareys, I. Razdobreev, Y. Shekun, J. Barrau, and J. C. Brabant, Superlatt. Microstruct. **12**, 7 (1992).

[28]C. Kittel, *Quantum Theory of Solids* (Wiley, New York, 1963).

[29]T. Takagahara, Phys. Rev. B **31**, 6552 (1985).

[30]J. Hegarty and M. R. Sturge, J. Opt. Soc. Am. B **2**, 1143 (1985).

[31]J. Feldmann, G. Peter, E. O. Göbel, P. Dawson, K. Moore, C. Foxon, and R. J. Elliott, Phys. Rev. Lett. **59**, 2337 (1987).

[32]M. Colocci, M. Gurioli, A. Vianetti, F. Fermi, C. Deparis, J. Massies, and G. Neu, Europhys. Lett. **12**, 417 (1990).